Sensors & Actuators: B. Chemical 336 (2021) 129704

Contents lists available at ScienceDirect

Sensors and Actuators: B. Chemical

journal homepage: www.elsevier.com/locate/snb

Ion sensitivity from current hysteresis in InAs nanowire field-effect transistors functionalized with ionophore-doped fluorosilicone membranes

Alex C. Tseng [a,b,1], Kensuke Ito [c], David Lynall [a,b], Igor G. Savelyev [a], Marina Blumin [a], Shiliang Wang [d], Harry E. Ruda [a,b], Toshiya Sakata [c,*]

[a] Centre for Advanced Nanotechnology, University of Toronto, 170 College Street, Toronto, Ontario M5S 3E4, Canada
[b] Department of Materials Science and Engineering, University of Toronto, 184 College Street, Toronto, Ontario M5S 3E4, Canada
[c] Department of Materials Engineering, School of Engineering, The University of Tokyo, 7-3-1 Hongo, Bunkyo-ku, Tokyo 113-8656, Japan
[d] Defence Research and Development Canada Suffield, Medicine Hat, Alberta T1A 8K6, Canada

ARTICLE INFO

Keywords:
InAs
Nanowire
Field-effect transistor
Hysteresis
Ionophore
Ion sensor

ABSTRACT

Trapping of environmental charges in surface states typically dominates electrical transport in nanostructured field-effect transistors (FETs) applied as sensors. Such surface effects produce exceptional sensitivity, yet time dependencies on experimental timescales simultaneously results in hysteresis of FET conductance and signal instability. Whereas hysteresis is usually suppressed by means of chemical surface treatments, here we study it as a source of information for ion sensing. Ion-sensitive FETs were prepared by coupling InAs nanowires to fluorosilicone membranes doped with Na^+ ionophores. From cyclic transfer characteristics in electrolytes of varying concentration, potentiometric and hysteretic calibration curves were obtained. The observed hysteresis was attributed to changes in membrane capacitance by redox reactions between ionized donor-like traps at the InAs surface and electroactive membrane constituents. Hysteresis was correlated to the ion potential through a model and demonstrated a filtering effect that stabilized the hysteretic response against potential drifts. Furthermore, the model elucidated the ability to modulate ion sensitivity by controlling the initial density of ionized traps via electrostatic polarization by the gate. In this mode of active operation, we demonstrate enhancement above the Nernstian limit with linear calibrations of (-77.5 ± 3.2 to -80.7 ± 3.0 mV/dec) despite the presence of non-equilibrium ion fluxes.

1. Introduction

Development of the next-generation of chemical and biological sensors with electrical read-outs increasingly targets field-effect transistors (FETs) employing nanostructured materials such as nanowires (NWs) and nanotubes [1,2]. By exposing the FET gate to the environment, the electric charge of adsorbed species is transduced and amplified as a current between source and drain electrodes (see Fig. 1a). Facile measurement is possible even as biosensors are miniaturized, contributing to its appeal in applications such as point-of-care diagnostics [3,4].

The prototypical biosensor is the ion-sensitive FET (ISFET) [5], and recent advancements have focussed on Si NWs [1,6]. This approach pairs well-studied Si chemistries (e.g. silanization [7,8]) with the benefits of nanostructure, such as enhanced sensitivity in FET sub-threshold regime [9] or geometric reduction of Debye screening [10]. However, a key challenge in developing NW biosensors is controlling the dominating influence of surface trap states on electrical transport [11]. This is often addressed by a passivating oxide [12]; for instance, the ideal NW biosensor modelled in Ref. [10] assumes no surface effects and expresses sensitivity in terms of the geometry (i.e. curvature) of the FET gate and electrical double layer capacitance.

Unfortunately, this view spurns information available from the interaction between surface states and analyte, which can manifest as random telegraph ($1/f$) noise when environmental charges are repeatedly exchanged with trap states [13,14]. Studies using this approach demonstrated enhanced limits of detection or sensitivity, albeit requiring sophisticated measurement schema not conducive towards *in situ* applications. Indeed, investigation of similar noise in our InAs NWFETs led to the realization of its exceptional charge sensitivity [15] and potential for biosensing.

* Corresponding author.
E-mail address: sakata@biofet.t.u-tokyo.ac.jp (T. Sakata).
[1] Present address: Department of Materials Engineering, School of Engineering, The University of Tokyo, 7-3-1 Hongo, Bunkyo-ku, Tokyo 113-8656, Japan.

https://doi.org/10.1016/j.snb.2021.129704
Received 30 October 2020; Received in revised form 16 February 2021; Accepted 20 February 2021
Available online 26 February 2021

The InAs surface intrinsically accumulates electrons, due to large surface state densities in a non-stoichiometric native oxide [16–18]. These states interact with adsorbed molecules, modulating electrical transport in InAs NWFETs, and have demonstrated applicability for sensing [19–21]. Furthermore, sensing of individual molecular dipoles at ultra-low concentrations has recently been demonstrated [22]. However, the trade-off for high sensitivity is again the dominating effect of surface states, which, in InAs, exhibit capture and emission rates on experimental timescales [23,24]. This produces hysteresis in measurements of FET current and is typically considered a problem to be eliminated. For instance, previous work on ISFETs using InAs NWs passivated the native oxide with Al_2O_3 and produced biosensors capable of detecting pH and protein charges [25].

In this study, rather than disparage hysteresis, we instead leverage it to obtain sensing responses to sodium cations (Na^+) that are more stable than the interface potential approximated by the FET threshold voltage (V_T). A model is developed to quantify NWFET current hysteresis and elucidate the origin of its ion sensitivity. The model reveals a key design parameter—the initial density of ionized trap states—which can enhance or suppress the sensitivity of the hysteretic response coupled to it. Experiments in simple electrostatic manipulation (i.e. polarization) of this parameter are presented as proof-of-concept for active operation of NW-ISFETs to modulate ion sensitivities.

2. Material and methods

InAs NWFETs were sensitized to Na^+ by coupling to fluorosilicone (FPS) polymer membranes uniformly doped with ionophores, similar to those used in ion-selective electrodes, shown schematically in Fig. 1. This semi-permeable membrane develops a potential localized at the polymer/electrolyte interface (ψ_{int}) dependent on Na^+ activity (a_{Na^+}) in the bulk solution that is described by the Nernst equation [26,27]:

$$\psi_{int} = 2.303\frac{RT}{F}log\frac{a_{Na^+,bulk}}{a_{Na^+,mem}} + \psi_o \quad (1)$$

where RT/F has its typical thermodynamic meaning, giving an ideal slope of 59.2 mV/decade of $a_{Na^+,bulk}$ at ambient. ψ_o encompasses the standard chemical potential, free energy change of complexation, and other system constants (e.g. junction potential). Therefore, ψ_{int} acts in series with a gating potential (V_{LG}) set by a reference/counter electrode (RE/CE). To better focus on NWFET hysteresis, Na^+ was chosen as a model analyte in conjunction with a well-established crown ether-based ionophore (bis(12-crown-4)) demonstrating Nernstian sensitivity [28]. The selectivity of this membrane system was previously evaluated with established protocols on thin-film InGaZnO ISFETs [29], and stability of Na^+ sensitivity upwards of 1 month was demonstrated on paper-based electrodes [30]. Further details are reported in the Supplementary Information (SI) §S1 and elsewhere for InAs NWFET [22] and ion-membrane [29] fabrication.

DC electrical characterization and sensing experiments were performed with either Keysight B1500A or Keithley 4200 analyzers, with source-measure units as dedicated channels for the drain electrode, RE/CE pair in a modified Kelvin probe configuration[2] [31], and back-gate electrode. The source electrode was connected to instrument ground. NWFETs operated in the linear regime by biasing the drain to $V_{DS} = 10$ mV and transfer curves (I_{DS} vs. V_{LG}) were measured by sweeping V_{LG} at a rate of ca. 30 mV/s via a Pt CE referenced to a Ag/AgCl in 3M $KCl_{(aq)}$ RE. The RE was connected to test solution through an agar gel salt bridge with its junction positioned within ca. 2 mm of the membrane/electrolyte interface. The back-gate was held constant at $V_{BG} = 0$ V. Photographs of the measurement apparatus can be seen in Fig. S1.

Devices employed in this study were firstly qualified by collecting transfer characteristics at major fabrication steps as described in SI §S1.4. In brief, suitable devices demonstrated minimal leakage currents and sufficient switching operation (viz. leakage current as 0.1% of I_{DS}, transconductance >10 μS and subthreshold swing <500 mV/dec) under electrolyte-gating. For analysis, V_T was extracted by extrapolating a least-squares fit of the linear region of a transfer curve to the abscissa.

Test solutions with [Na^+] ranging from 5 mM to 1000 mM were buffered with 20 mM HEPES at physiological pH ~7.3 to control for the impact of H^+ activity and preparation is described in SI §S1.3. In sensing experiments, 10 μL aliquots of solution were dispensed by micro-pipette and measurements proceeded in order of increasing then decreasing [Na^+]. Test solutions were exchanged four times for every step of [Na^+], with the fourth aliquot used to collect a transfer curve. Additionally, the tips of RE and CE were wetted during exchanges to mitigate any residues. Solutions remained in contact with the membrane for 2 min with $V_{LG} = 0$ V prior to a measurement, taken 3 times per step, of which the final is reported. To electrostatically manipulate ionized trap state density, NW-ISFETs were polarized by biasing V_{LG} at the starting potential of a sweep during the solution contact time.

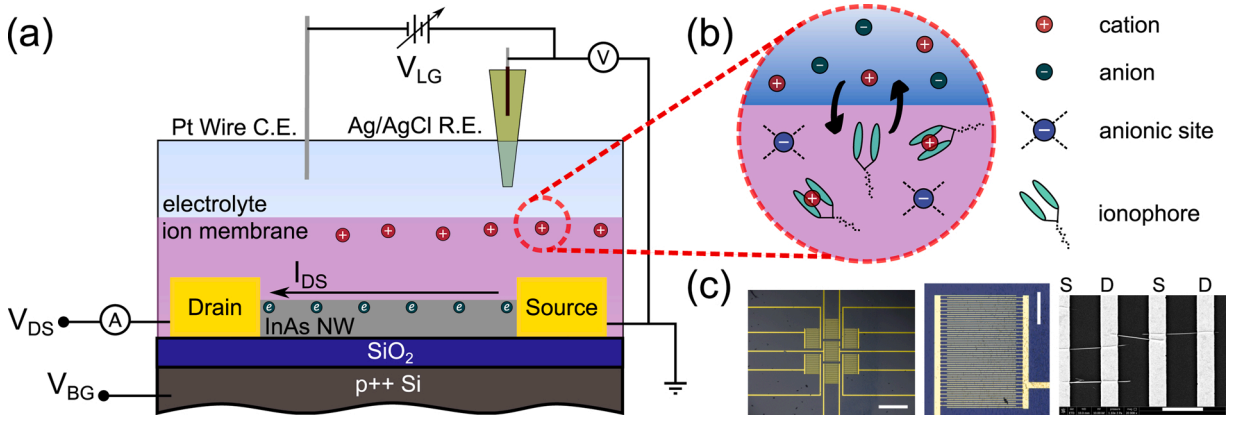

Fig. 1. (a) Schematic diagram of an InAs NWFET coupled with ion-selective FPS membrane and electrical connections. (b) Magnification of ion-selective FPS membrane. Complexation is represented by arrows to/from a cation and ionophore species. (c) Left to right: optical, optical, and SEM micrographs of an InAs multi-NWFET array with alternating source (S) and drain (D) contacts. Scale bars are 500 μm, 100 μm and 5 μm, respectively.

[2] The RE serves as the potential sensing contact, while the CE is used to force current.

3. Results and discussion

3.1. Quantified hysteresis model

Data from a representative Na^+ sensing experiment without polarization are shown in Fig. 2. The transfer curves in Fig. 2a, b are characteristic of the n-type NW-ISFETs fabricated from our InAs NWs under electrolyte-gating and I_{DS} hysteresis is observed in their lineshape. For comparison, Fig. S3 shows data before and after membrane deposition. Generally, upward (i.e. $dV_{LG}/dt > 0$) sweeps showed smaller I_{DS} regardless of whether the sweep led or trailed. Thus, hysteresis in these electrolyte-gated, membrane-coupled InAs NW-ISFETs possesses an anti-clockwise character, contrasting with previous observations of back-gated devices with native oxide surfaces in vacuum and air (i.e. clockwise) [23,24].

Investigations of electrolyte-gated, ambipolar graphene FETs [32] attributed such anti-clockwise I_{DS} hysteresis to the charging of the electrical double layer capacitor (C_{DL}) by the gate electrode. For instance, at the turning point of the transfer measurement after applying positive electric field, the region near the FET gate interface is enriched in cations, resulting in increased I_{DS} (i.e. due to compensated carrier density in n-type devices). In our NWFETs, the leakage current (i.e. I_{LG}) data in Fig. S3 demonstrates this capacitive charging by its lineshape (i.e. with minimal electrochemical interference) and a magnitude of integral capacitance (estimated by the injected charge and geometric area in solution contact, $C = \int I_{LG}\, dt \cdot A^{-1}(\max V_{LG} - \min V_{LG})^{-1}$) on the order of 10^{-5} F/cm^2 (cf. 2 to 8×10^{-5} F/cm^2 for typical electrical double layers [33]). Note that for analyte charges localized in the membrane layer C_{DL} is considered to be in parallel [10] with the gate capacitance stack (C_g as defined in §S2.1), and thus the magnitude of C_{DL} dominates coupling of applied potentials to carrier density in the NW (alternatively, the effect of adsorbed charges at the NW/electrolyte interface on the potential in the channel).

Hence, idealized models of NWFET ion sensitivity often forego consideration of changes to C_g, which for our devices is essentially the series capacitance of the InAs native oxide and ion-membrane stack. Note that we neglect the NW quantum capacitance as NWFETs are operated in the linear regime and InAs is intrinsically accumulating. However, in comparing transfer curves and leakage current data before and after membrane deposition it is obvious that capacitive charging cannot fully account for the I_{DS} hysteresis observed in Fig. 2a, b. That is, I_{DS} lineshape is significantly altered despite qualitatively and quantitatively similar leakage current behaviour. This indicates that the InAs surface state distribution is altered, but not passivated, by the deposition of FPS ion-membranes. Therefore, understanding how the NW potential (and FET conductance) is affected by analyte charges (i.e. NW-ISFET sensitivity) requires tracking the population of surface states at the interior NW/membrane interface in tandem with C_g.

Qualitatively, we consider the interaction between donor-like InAs surface states and tetraorganoborate anionic sites in the membrane. Incorporated from sodium salts, these borates possess a negative charge and set the NWFET in enhancement-mode (i.e. positive V_T). Subsequent lowering of energy band levels in the channel by raising V_{LG} provides an overpotential and drives oxidation of borates into stable neutral radicals [34,35], with ionized donors acting as oxidizing agents. At this interface, the neutralization of positive donors at the NW surface and negative borates in the membrane effectively reduces the electric dipole density in the gate capacitor, consequently decreasing permittivity and hence C_g.

In other words, an electrochemical interaction at the NW/membrane interface can be modelled as a negative differential (pseudo-)capacitance (NDC) in parallel with C_g. This is similar to NDC observed at room-temperature in InAs quantum heterostructures and attributed to the charging/discharging of carriers in confined states by measurement perturbation [36]. A similar model has also been used to explain I_{DS} hysteresis arising from NDC in so-called solid electrolyte FETs [37]. In these devices, sweeping the gate potential causes the drift and diffusion of mobile oxygen ions and corresponding vacancies in an oxide membrane used as the gate dielectric on oxide semiconductor channels. The frequency dependence of this ion migration polarizes the semiconductor/membrane interface and gives rise to NDC. In contrast, Na^+-ionophore complexes in our ion-membranes limit the mobility of ionic species, leading us to propose an electrochemical mechanism for the NDC observed here.

From Fig. 2a, b, we observe that this decrease of C_g dominates any reduction in ionized impurity scattering from neutralization of charges as lower transconductance ($g_m \equiv dI_{DS}/dV_{LG}$) is generally seen in downward transfer sweeps. This decreased slope results in ΔV_T as V_{LG} is swept

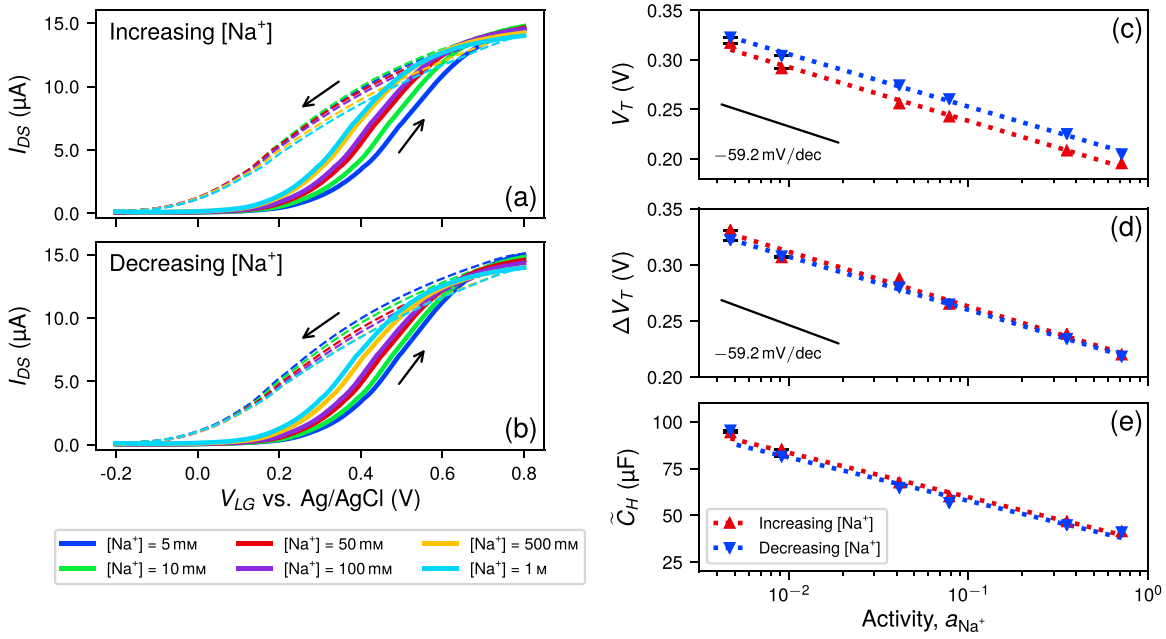

Fig. 2. Transfer curves of an un-polarized InAs NW-ISFET with $V_{DS} = 10$ mV and (a) increasing or (b) decreasing [Na^+] in solution. Arrows indicate the direction and solid (dashed) lines represent the leading (trailing) half of the sweep. Corresponding calibration curves extracted from (c) threshold voltage of the leading sweep, (d) threshold voltage shift between sweeps, and (e) hysteresis quasi-capacitance. Dashed lines are linear fits and serve as a guide to the eye. Error bars larger than data markers represent measurement uncertainty in activity (horizontal) or standard error in extracted parameters (vertical). Ideal Nernst slopes for Na^+ at ambient are annotated in (c) and (d).

back from its turning point. We associate this potential change with an induced hysteresis charge (ΔQ_f) within the gate stack and its amount depends on the competition between borate oxidation and simple electron capture into donor-like traps caused by sweeping V_{LG}. Therefore, ΔV_T drops over both C_{DL} and C_g, and while tracking changes to C_g we can use a description of the flat-band voltage of an ISFET [33] to show:

$$\Delta V_T \equiv V_{T,\mathrm{up}} - V_{T,\mathrm{down}} = -\Delta\left(\frac{Q_f}{C_g}\right) = \frac{\alpha\Delta Q_f + (\alpha-1)Q_{f,\mathrm{up}}}{C_{g,\mathrm{up}}} \quad \text{where } \Delta Q_f = Q_{f,\mathrm{down}} - Q_{f,\mathrm{up}} \text{ and } \alpha = \frac{C_{g,\mathrm{up}}}{C_{g,\mathrm{down}}} \tag{2}$$

wherein other contributions to the flat-band voltage are assumed constant—typical when approximating ψ_{int} by V_T—except the net density of "fixed" charges ($Q_f = e(N_+ - N_-)$, where N is the number density of positive or negative charge). The history dependence of C_g between sweeps is simplified as α, which is reasonable and discussed further in SI §S2.1. A negative sign arises algebraically and tracks the shift direction. Although the contribution of ψ_{int} is directly eliminated by differencing of V_T, its effect is preserved in the range of V_{LG} (i.e. $V_{LG,\mathrm{eff}} = V_{LG} + \psi_{\mathrm{int}}$) and manifests indirectly in the oxidation overpotential and the driving force for capture and emission into trap states. Given fast rates of complexation, varying ψ_{int} via [Na^+] of test solutions can thus be considered as probing these two processes.

The latter process determines the filling of ionized donors by trapping, which is thus proportional to the interface charge due to Na^+ ions (Q_{int}). Furthermore, the total amount of neutralized charge is the sum of filled donors and ΔQ_f, and is itself proportional to the initial density of ionized donors ($Q_{f,\mathrm{up}}$) available to be neutralized. Therefore, when oxidation and trapping occur on similar timescales, the induced hysteresis charge can be seen as a reflection of the interface charge mirrored in trap states (i.e. $\Delta Q_f \propto \gamma Q_{f,\mathrm{up}} - Q_{\mathrm{int}}$). This relationship is evidenced in Fig. 2d, for monotonically decreasing, positive ΔV_T with increasing a_{Na^+}.

This view of ΔQ_f inspires another quantification of I_{DS} hysteresis as charge injected into the gate dielectric. To calculate total charge 1(i.e. disregarding sign), we take the unsigned area enclosed between transfer sweeps:

$$A_H \equiv \int_{V_{\mathrm{min}}}^{V_{\mathrm{max}}} \left| I_{\mathrm{DS,down}} - I_{\mathrm{DS,up}} \right| \mathrm{d}V_{\mathrm{LG}} \tag{3}$$

It is obvious that this integral does not directly correspond to injected charge, because I_{DS} is modulated by V_{LG} via a transfer characteristic. Thus, a model for I_{DS} of a NWFET in the linear regime [38] is required to evaluate the integral:

$$I_{\mathrm{DS}} = \frac{\mu_{\mathrm{FE}} C_g}{L^2}\left(V_{\mathrm{GS}} - V_T - \frac{V_{\mathrm{DS}}}{2}\right)V_{\mathrm{DS}} = g_m\left(V_{\mathrm{GS}} - V_T - \frac{V_{\mathrm{DS}}}{2}\right) \tag{4}$$

where $V_{GS} = V_{LG}$ and device properties such as field-effect mobility (μ_{FE}), channel length (L), and C_g (including the radial dependence of these quantities) can be aggregated in g_m. Therefore:

$$A_H = (V_{\mathrm{max}} - V_{\mathrm{min}})[g_{m,\mathrm{up}}(V_{T,\mathrm{up}} - V_\beta) - g_{m,\mathrm{down}}(V_{T,\mathrm{down}} - V_\beta)] \quad \text{where } V_\beta = (V_{\mathrm{max}} + V_{\mathrm{min}} - V_{\mathrm{DS}})/2 \tag{5}$$

Previous studies of these InAs NWs [38] showed that, even at room temperature, μ_{FE} is inversely proportional to surface charge density as ionized impurity scattering dominates (i.e. $\mu_{FE} \propto 1/Q_f$). Therefore, $g_m \propto C_g/Q_f$, and (5) gives:

$$A_H \propto (V_{\mathrm{max}} - V_{\mathrm{min}})(V_T' - V_\beta)\cdot\Delta\left(\frac{C_g}{Q_f}\right)$$

$$\Delta\left(\frac{C_g}{Q_f}\right) = \frac{C_{g,\mathrm{up}}}{Q_{f,\mathrm{up}}}\left[1 + \frac{Q_{f,\mathrm{up}}}{\alpha\Delta Q_f + (\alpha-1)Q_{f,\mathrm{up}}}\right]^{-1} = \frac{C_{g,\mathrm{up}}}{Q_{f,\mathrm{up}}}\left[1 + \frac{Q_{f,\mathrm{up}}}{\Delta V_T \cdot C_{g,\mathrm{up}}}\right]^{-1} \tag{6}$$

where, as in (2), V_T' represents the assumed constant contributions to the flat-band voltage and ΔQ_f and α are defined. When $|\Delta V_T \cdot C_{g,\mathrm{up}}| \ll |Q_{f,\mathrm{up}}|$, (6) can be simplified:

$$A_H \propto (V_{\mathrm{max}} - V_{\mathrm{min}})(V_T' - V_\beta)\left(\frac{C_{g,\mathrm{up}}}{Q_{f,\mathrm{up}}}\right)^2 \Delta V_T \tag{7}$$

This inequality is confirmed empirically in Fig. 3 by observed linearity between A_H and ΔV_T throughout all studied polarization regimes for a representative and alternative device. As elaborated in SI §S2.2, this relation holds because of large surface state densities in InAs. It is now apparent that, like ΔV_T, A_H is dependent on Q_{int} through ΔQ_f.

As a non-equilibrium quantity, ΔQ_f is dependent on the dynamic parameters of the measurement: the range of V_{LG}—practically limited by minimizing electrochemical interference—and on dV_{LG}/dt—initially chosen to probe the response of faster trap states [24] more relevant for sensing. dV_{LG}/dt also dictates the balance between the rates of borate oxidation versus simple electron capture into traps. Thus, normalizing A_H by these parameters (i.e. $\widetilde{C}_H \equiv A_H\left(\frac{\mathrm{dV_{LG}}}{\mathrm{dt}}(maxV_{\mathrm{LG}} - minV_{\mathrm{LG}})\right)^{-1}$amounts to a change of variable in (3) and elimination of the first term in (5), leaving units of capacitance. We term the resulting quantity ($\widetilde{C}_H$) as hysteresis quasi-capacitance, which describes how the observed change in carrier density, modulated by μ_{FE}, in the NWFET channel by the sweeping action of V_{LG} is related to ΔQ_f. We represent the data in this form as it is useful to think of I_{DS} hysteresis in terms of stored charge.

Furthermore, the extensivity of $\widetilde{C}_H$ (cf. I_{DS}) must be contained in the remaining pre-factors of (7), inasmuch as ΔV_T is intensive because terms in (2) scale by the same factors (e.g. number of NWs, active surface area, etc.). Hence, using regression slopes from Fig. 3 as proportionality constants to restate $\widetilde{C}_H$ sensitivity in potential terms aids the comparison of experimental results and the Nernstian ideal (i.e. left-hand side of (8)). Accordingly, the magnitude of $\widetilde{C}_H$ and its relationship to ΔV_T is associated with the set of dynamic parameters used to obtain the data. In the present study, we maintained these settings as a constant to allow for calibration of $\widetilde{C}_H$ sensitivity throughout polarization regimes. Fig. 2c–e show Na^+ calibration data for un-polarized NW-ISFETs extracted from V_T of the leading sweep, ΔV_T, and $\widetilde{C}_H$, respectively. Fit parameters for all presented data are given in Table 1.

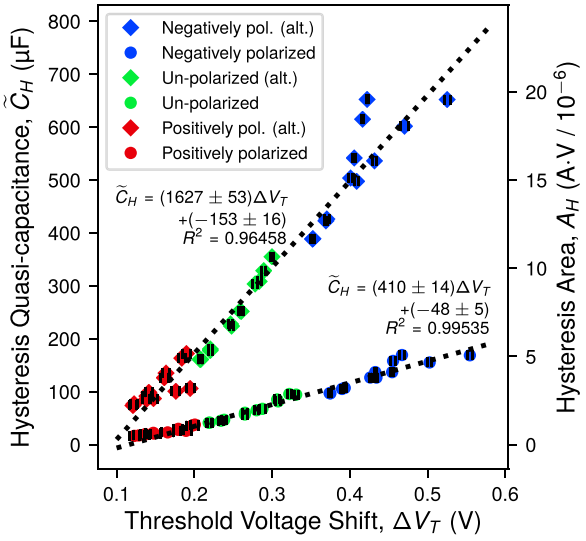

Fig. 3. Hysteresis quasi-capacitance (area) vs. threshold voltage shift for two InAs NW-ISFETs under various polarization conditions. Horizontal error bars represent standard error in extracted ΔV_T. Dashed lines show a least squares fit with annotated fit parameters.

3.2. Un-polarized InAs NW-ISFET calibrations

Un-polarized V_T sensitivity is close to the Nernstian ideal (ca. −54 mV/dec) and in excellent agreement with our previous work on this FPS membrane [29], in addition to reports of bis(12-crown-4) in other systems [39,40]. However, a vertical shift between regression lines for increasing and decreasing [Na^+] in Fig. 2c is apparent, indicating poor stability of the V_T response and concomitant loss of calibration accuracy. These potential shifts were observed, regardless of membrane pre-conditioning, in both InAs NW and planar Si ISFETs (see Fig. S5, Table S2) suggesting the source of the error as a slow net electrophoresis of Na^+ into/from the membrane by applied V_{LG}. Assuming that $a_{Na^+,mem}$ is no longer constant in (1), a relative change can be calculated using the similar regression slopes and change in intercept (ca. 16 mV). The result reveals a near doubling of $a_{Na^+,mem}$ as the sensing experiment proceeds, with the same ratio representing the accuracy loss.

In contrast, calibrations of ΔV_T and $\widetilde{C}_H$ (Fig. 2d, e) are stable with no significant shift. This arises from differencing in (2) and (3), as errors from symmetric (i.e. slow) potential drifts apply equally to both halves of a sweep and cancel out. Stable responses in V_T, referenced to the RE potential, cannot accommodate these drifts that are likely when [Na^+] changes through orders of magnitude. This illustrates the reduced first-order errors in hysteretic responses, as each datum is derived from changes to the NWFET surface in its immediate context. In this way, the hysteresis quasi-capacitance is akin to a high-pass filter and attenuates the signal from slow electrophoretic drifts.

However, ΔV_T sensitivity (ca. −48 mV/dec) is decreased by about 10% compared to V_T. As near-Nernstian sensitivities were observed in V_T, this suggests that mirroring of Q_{int} into trap states is likely incomplete at measurement timescales and dynamic parameters may yet be optimized. Indeed, $V_{T,down}$ exhibits small a_{Na^+} dependency (ca. −6 mV/dec), indicating that ΔV_T has some additional unaccounted dependence. This is a higher-order error related to trap dynamics. In comparison, converted potentiometric sensitivities for the $\widetilde{C}_H$ response (−57.8 ± 3.5 and −56.6 ± 5.6 mV/dec for increasing and decreasing [Na^+], respectively) return to Nernstian values. Moreover, as Fig. S7 shows, the $\widetilde{C}_H$ response is remarkably stable, maintaining sensitivity after storage periods of two weeks to two months in ambient conditions.

It is likely that an unnamed pre-factor in (7) holds an inverse dependence related to the higher-order error in ΔV_T. In fact, theoretical A_H by (5) is an overestimate of observed A_H (Fig. S4a) as non-ideality is neglected (e.g. mobility degradation by surface or self scattering at increased carrier densities). Contrasting Fig. 3 with theoretical A_H vs. ΔV_T (Fig. S4b) illustrates that the observed linearity across polarization regimes is attributable to non-ideality. This is elucidated by partial differentiation of (7):

$$\begin{aligned}\frac{\partial A_H}{\partial a_{Na^+}}\left(\frac{\partial A_H}{\partial \Delta V_T}\right)^{-1} &= \frac{\partial \Delta V_T}{\partial a_{Na^+}} + \left\{\left[\frac{\Delta V_T}{V_T' - V_\beta}\right]\frac{\partial V_T'}{\partial a_{Na^+}} - 2\left[\frac{\Delta V_T \cdot C_{g,up}}{Q_{f,up}}\right]\frac{\partial (Q_{f,up}/C_{g,up})}{\partial a_{Na^+}}\right\} \\ &= \frac{\partial \Delta V_T}{\partial a_{Na^+}} - \left\{\left[\frac{\Delta V_T}{V_T' - V_\beta}\right]\frac{\partial \psi_{int}}{\partial a_{Na^+}} + 2\left[\alpha\frac{Q_{f,down}}{Q_{f,up}} - 1\right]\frac{\partial (Q_{f,up}/C_{g,up})}{\partial a_{Na^+}}\right\}\end{aligned} \tag{8}$$

where $\partial A_H/\partial \Delta V_T$ contains unnamed proportionality factors and (2) has been substituted in the second expression. Terms in curly braces are named factors that modulate A_H sensitivity. Assuming that solvated ions are unable to dope InAs, the activity dependence of V_T' is simply the Nernst sensitivity from (1). However, with $|\Delta V_T \cdot C_{g,up}| \ll |Q_{f,up}|$ and $V_T = V_T' - \frac{Q_f}{C_g}$, both terms in square braces will approach zero. Note, typically $V_T \sim V_\beta$, as the measurement range (represented by V_β) is chosen to best capture the transfer curve. Therefore, the influence of these terms is similarly small (ca. 0.1%, see SI §S2.2) and it is likely that an unnamed factor accounts for $\widetilde{C}_H$ sensitivity that approaches ideal values in the un-polarized case.

Table 1
Fit parameters of presented calibration data.

Curve	[Na^+] direction	Slope	Intercept	R^2
Un-polarized NW-ISFET (Fig. 2)				
V_T	Increasing	−54.3 ± 2.3 mV/dec	184 ± 3 mV	0.99647
	Decreasing	−53.0 ± 1.4 mV/dec	200 ± 2 mV	0.99783
ΔV_T	Increasing	−48.8 ± 2.7 mV/dec	214 ± 4 mV	0.99078
	Decreasing	−47.4 ± 0.7 mV/dec	213 ± 1 mV	0.99928
$\widetilde{C}_H$	Increasing	−23.7 ± 1.2 μF/dec	36.1 ± 1.6 μF	0.99426
	Decreasing	−23.2 ± 2.2 μF/dec	34.6 ± 2.7 μF	0.98586
Negatively polarized NW-ISFET (Fig. 4)				
V_T	Increasing	−92.0 ± 5.7 mV/dec	170 ± 5 mV	0.99855
	Decreasing	−68.5 ± 5.7 mV/dec	184 ± 6 mV	0.96864
ΔV_T	Increasing	−69.7 ± 4.9 mV/dec	362 ± 5 mV	0.99465
	Decreasing	−45.2 ± 3.2 mV/dec	371 ± 3 mV	0.98304
$\widetilde{C}_H$	Increasing	−31.8 ± 0.8 μF/dec	92.3 ± 0.9 μF	0.99930
	Decreasing	−33.1 ± 0.6 μF/dec	90.9 ± 0.7 μF	0.99939

NB: Additional calibrations for other devices and polarizations presented in Table S2.

3.3. Polarized InAs NW-ISFET calibrations

Nonetheless, (8) reveals a basis for modulation of the A_H ($\widetilde{C}_H$) response: while the first term in curly braces is coupled to the Nernst sensitivity and thus constant, the second is coupled to $Q_{f,up}$ and, critically, its dependence on a_{Na^+}, which may be externally manipulated. This is simply achieved by electrostatic polarization via V_{LG} or V_{BG}. Here, V_{LG} is used as timing is more readily coordinated by holding a pre-sweep bias as compared to switching potential sources. However, V_{BG} may allow greater ranges as it is insulated from the electrolyte. In either case, the membrane composition will change simultaneously due to electrophoresis dependent on the applied potential, hold time, and bulk [Na^+]. In this actively operated regime, the capacity to filter out first-order errors enables extraction of useful information.

Data showing sensitivity enhancement is given in Fig. 4. With negative polarization of $V_{LG} = -200$ mV, the channel level is raised, increasing the rate of donor ionization and $Q_{f,up}$. This also enhances the magnitude of $\partial(Q_{f,up}/C_{g,up})/\partial a_{Na^+}$, as level raising by $V_{LG,eff}$ is less for larger [Na^+]. Simultaneously, the ion-membrane is pushed out of equilibrium into a Na^+ depleted state. The resulting gradient drives additional diffusive flux of Na^+ into the membrane during measurements, producing the observed super-Nernstian responses [41] in V_T (Fig. 4c).

Moreover, differences in transfer curve lineshape between Fig. 4a, b and significant hysteresis in V_T sensitivity clearly demonstrate that contributions from non-equilibrium ion fluxes are strongly dependent on initial conditions. After filtering out slow potential drifts by ΔV_T (Fig. 4d), sensitivity similar to the un-polarized state (ca. −45 mV/dec) is obtained in the decreasing [Na^+] run. However, the increasing run remains super-Nernstian, corresponding to asymmetric (i.e. fast)

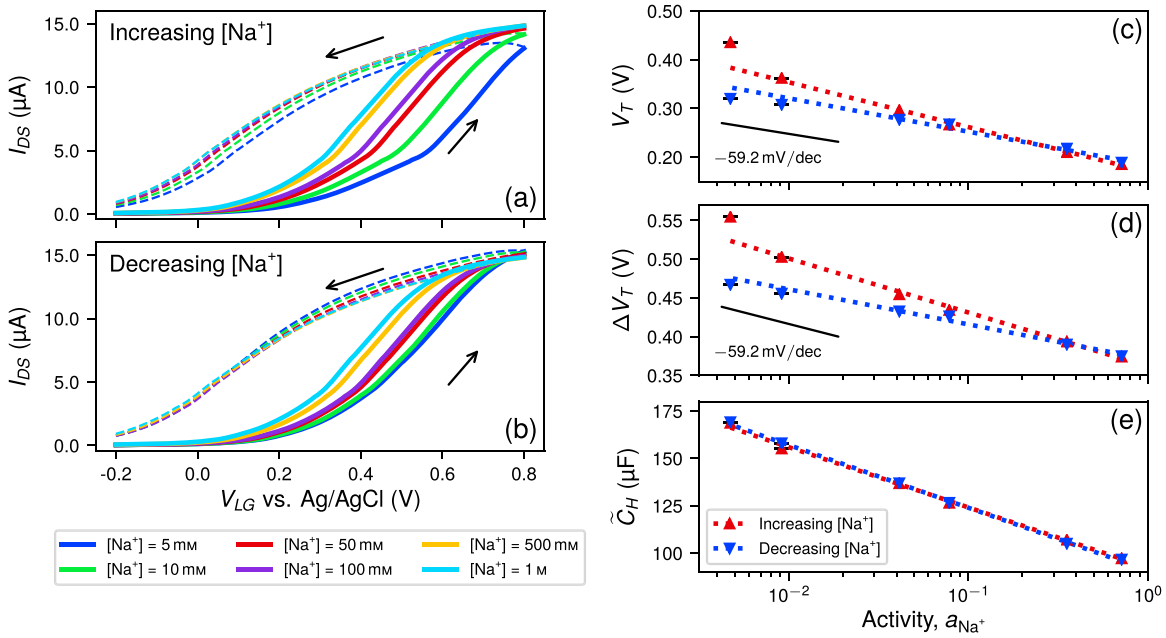

Fig. 4. Transfer curves of a negatively polarized InAs NW-ISFET with $V_{DS} = 10$ mV and (a) increasing or (b) decreasing [Na^+] in solution. Arrows indicate the direction and solid (dashed) lines represent the leading (trailing) half of the sweep. Corresponding calibration curves extracted from (c) threshold voltage of the leading sweep, (d) threshold voltage shift between sweeps, and (e) hysteresis quasi-capacitance. Dashed lines are linear fits and serve as a guide to the eye. Error bars larger than data markers represent measurement uncertainty in activity (horizontal) or standard error in extracted parameters (vertical). Ideal Nernst slopes for Na^+ at ambient are annotated in (c) and (d).

potential shifts from a net injection of Na^+ into the membrane by sweeping V_{LG}. This is further evidenced by shifting of $V_{T,\mathrm{down}}$ in these runs. From about 50 mM Na^+ onwards, a quasi-equilibrium is reached and these shifts disappear.

Accordingly, ΔQ_f in these runs is lower than expected for the observed value of ΔV_T as part of applied V_{LG} rather works to inject charge as Na^+. Hence, $\partial(Q_{f,\mathrm{up}}/C_{g,\mathrm{up}})/\partial a_{Na^+}$ is smaller in these initial data. That is, sections of the ΔV_T response that experience additional potential shifts from non-equilibrium ion fluxes realize less sensitivity enhancement in terms of $\widetilde{C}_H$ (Fig. 4e) and the resulting non-linear behaviour equalizes the calibration slopes (-77.5 ± 3.2 and -80.7 ± 3.0 mV/dec for increasing and decreasing [Na^+], respectively), which is enhanced by about 40% over the un-polarized state.

The expected degree of $\widetilde{C}_H$ sensitivity enhancement from coupling to $\partial(Q_{f,\mathrm{up}}/C_{g,\mathrm{up}})/\partial a_{Na^+}$ can be estimated using the spectral density of surface states near the conduction band edge in these InAs NWs (cf. $10^{12}\,\mathrm{cm^{-2}\,eV^{-1}}$) [38], assuming strong coupling of $V_{LG,\mathrm{eff}}$ to the energy level of the channel—reasonable given the range of V_{LG} and observed transfer characteristics. In conjunction with estimated C_g (see SI §S2.1), this value is suitably large to overcome the minimizing term in (8), giving enhancement on the order of 10 mV/dec in agreement with the observed $\widetilde{C}_H$ response.

The fact that neither stability nor true sensitivity enhancement is observed in the ΔV_T response emphasizes the significance of coupling to the initial density of ionized traps to produce modulation of $\widetilde{C}_H$ sensitivity. For instance, the reverse effect of suppression occurs if the signs of the modulating factors in (8) are mismatched. This was observed when acceptor-like traps were activated by positive polarization of InAs NW-ISFETs (see SI §S3.2). Ultimately, ΔQ_f is a mirror of Q_{int} and subject to the same thermodynamic limits. However, directly coupling the sensor response to trap states allows for sensitivity modulation by the active operation of NW-ISFETs. Our success in demonstrating the proof-of-concept points towards the need for a deeper understanding of the trap state distribution—and ways to engineer it—in nanostructured sensors to further optimize this modulation effect.

4. Conclusions

Using InAs NWs coupled to polymeric ion-selective membranes as ISFETs to sense Na^+, we showed that potentiometric sensitivities derived from quantified current hysteresis (ΔV_T and $\widetilde{C}_H$) are more stable than the commonly used V_T, which tracks the potential due to ions at the membrane/electrolyte interface. We show how these data may be readily gleaned from FET transfer characteristics, provided that consistent dynamic parameters are maintained and the gate potential is applied in a closed loop. We developed a model that elucidated the origin of ion sensitivity in current hysteresis as the mirroring of interfacial charges into surface trap states. Greater stability—in terms of repeatability against potential drifts caused by variation in membrane composition—was achieved because the mirrored charges were counted by the *change* of ionized trap density, effectively acting as a filter to reduce first-order errors.

The model further revealed that the $\widetilde{C}_H$ response is coupled to the initial density of ionized traps in a manner that allows external manipulation, giving a basis for the active operation of NW-ISFETs to modulate sensitivity. This concept was proved by simple electrostatic polarization via applied V_{LG}, whereby energy bands in the InAs NW channel are repositioned for a time to enhance variation in the initial density of ionized traps with the interfacial potential. Meanwhile, the direction of modulation is largely controlled by the role of ionized traps in determining the capacitance of the NW/membrane interface. Both enhancement and suppression effects were observed, in accordance with the type of traps at play—donors and acceptors, respectively. In either case, active operation drives both electronic and ionic charges into non-equilibrium, producing significant errors in the V_T response. However, the stability of hysteretic responses means extraction of meaningful sensing information remains possible.

Here, we explored the implications of the model experimentally in InAs NW-ISFETs thanks to the existence of both donor and acceptor-like trap states and favourable alignment of energy bands with the operating range and timescale of V_{LG}. However, we emphasize that this result is general to FET sensors with trap states in communication with the

semiconductor channel and that significantly modulate electronic transport by ionized scattering, as is commonly the case with nanostructured devices. In the field of FET-based sensing, much effort is spent on isolating the effect of ψ_{int}, sometimes at the expense of so-called confounding factors like traps, whereas our results illustrate that FET hysteresis can be taken as an information source and gives a physical basis for overcoming the Nernstian limit in potentiometric sensors.

Author contributions

Alex C. Tseng: Investigation, methodology, writing – original draft. Kensuke Ito: Investigation, methodology. David Lynall: Methodology, writing – review & editing. Igor G. Savelyev: Resources. Marina Blumin: Resources. Shiliang Wang: Conceptualization, writing – review & editing. Harry E. Ruda: Conceptualization, supervision, writing – review & editing. Toshiya Sakata: Conceptualization, supervision, writing – review & editing.

Conflict of interest

The authors declare that there is no conflict of interest.

Declaration of Competing Interest

The authors report no declarations of interest.

Acknowledgements

Portions of this work were supported by the Natural Sciences and Engineering Research Council of Canada (NSERC), Defence Research and Development Canada (DRDC), and the Mirai Program of Japan Science and Technology (JST). Particularly, A.C.T. acknowledges the Michael Smith Foreign Study Supplement from NSERC for funding an exchange to Sakata Laboratory.

Appendix A. Supplementary data

Supplementary data associated with this article can be found, in the online version, at https://doi.org/10.1016/j.snb.2021.129704.

References

[1] A. Zhang, C.M. Lieber, Nano-bioelectronics, Chem. Rev. 116 (1) (2015) 215–257, https://doi.org/10.1021/acs.chemrev.5b00608.
[2] M. Kaisti, Detection principles of biological and chemical FET sensors, Biosens. Bioelectron. 98 (2017) 437–448, https://doi.org/10.1016/j.bios.2017.07.010.
[3] T. Sakata, Biologically coupled gate field-effect transistors meet in vitro diagnostics, ACS Omega 4 (7) (2019) 11852–11862, https://doi.org/10.1021/acsomega.9b01629.
[4] N. Shehada, J.C. Cancilla, J.S. Torrecilla, E.S. Pariente, G. Brönstrup, S. Christiansen, D.W. Johnson, M. Leja, M.P.A. Davies, O. Liran, N. Peled, H. Haick, Silicon nanowire sensors enable diagnosis of patients via exhaled breath, ACS Nano 10 (7) (2016) 7047–7057, https://doi.org/10.1021/acsnano.6b03127.
[5] P. Bergveld, Development of an ion-sensitive solid-state device for neurophysiological measurements, IEEE Trans. Biomed. Eng. 17 (1) (1970) 70–71, https://doi.org/10.1109/tbme.1970.4502688.
[6] L. Mu, Y. Chang, S.D. Sawtelle, M. Wipf, X. Duan, M.A. Reed, Silicon nanowire field-effect transistors—a versatile class of potentiometric nanobiosensors, IEEE Access 3 (2015) 287–302, https://doi.org/10.1109/access.2015.2422842.
[7] N. Gao, W. Zhou, X. Jiang, G. Hong, T.-M. Fu, C.M. Lieber, General strategy for biodetection in high ionic strength solutions using transistor-based nanoelectronic sensors, Nano Lett. 15 (3) (2015) 2143–2148, https://doi.org/10.1021/acs.nanolett.5b00133.
[8] G. Presnova, D. Presnov, V. Krupenin, V. Grigorenko, A. Trifonov, I. Andreeva, O. Ignatenko, A. Egorov, M. Rubtsova, Biosensor based on a silicon nanowire field-effect transistor functionalized by gold nanoparticles for the highly sensitive determination of prostate specific antigen, Biosens. Bioelectron. 88 (2017) 283–289, https://doi.org/10.1016/j.bios.2016.08.054.
[9] X.P.A. Gao, G. Zheng, C.M. Lieber, Subthreshold regime has the optimal sensitivity for nanowire FET biosensors, Nano Lett. 10 (2) (2010) 547–552, https://doi.org/10.1021/nl9034219.
[10] K. Shoorideh, C.O. Chui, On the origin of enhanced sensitivity in nanoscale FET-based biosensors, Proc. Natl. Acad. Sci. U. S. A. 111 (14) (2014) 5111–5116, https://doi.org/10.1073/pnas.1315485111.
[11] J. Jie, W. Zhang, K. Peng, G. Yuan, C.S. Lee, S.-T. Lee, Surface-dominated transport properties of silicon nanowires, Adv. Funct. Mater. 18 (20) (2008) 3251–3257, https://doi.org/10.1002/adfm.200800399.
[12] O. Knopfmacher, A. Tarasov, W. Fu, M. Wipf, B. Niesen, M. Calame, C. Schönenberger, Nernst limit in dual-gated Si-nanowire FET sensors, Nano Lett. 10 (6) (2010) 2268–2274, https://doi.org/10.1021/nl100892y.
[13] G. Zheng, X.P.A. Gao, C.M. Lieber, Frequency domain detection of biomolecules using silicon nanowire biosensors, Nano Lett. 10 (8) (2010) 3179–3183, https://doi.org/10.1021/nl1020975.
[14] J. Li, S. Pud, M. Petrychuk, A. Offenhäusser, S. Vitusevich, Sensitivity enhancement of Si nanowire field effect transistor biosensors using single trap phenomena, Nano Lett. 14 (6) (2014) 3504–3509, https://doi.org/10.1021/nl5010724.
[15] J. Salfi, I.G. Savelyev, M. Blumin, S.V. Nair, H.E. Ruda, Direct observation of single-charge-detection capability of nanowire field-effect transistors, Nat. Nanotechnol. 5 (10) (2010) 737–741, https://doi.org/10.1038/nnano.2010.242.
[16] M. Noguchi, K. Hirakawa, T. Ikoma, Intrinsic electron accumulation layers on reconstructed clean InAs(100) surfaces, Phys. Rev. Lett. 66 (17) (1991) 2243–2246, https://doi.org/10.1103/physrevlett.66.2243.
[17] J.R. Weber, A. Janotti, C.G.V. de Walle, Intrinsic and extrinsic causes of electron accumulation layers on InAs surfaces, Appl. Phys. Lett. 97 (19) (2010) 192106, https://doi.org/10.1063/1.3518061.
[18] N. Tomaszewska, L. Walczak, J. Lis, J.J. Kolodziej, Surface states and charge accumulation states on reconstructed InAs(001) surfaces, Surf. Sci. 632 (2015) 103–110, https://doi.org/10.1016/j.susc.2014.09.019.
[19] A.C. Tseng, D. Lynall, I. Savelyev, M. Blumin, S. Wang, H. Ruda, Sensing responses based on transfer characteristics of InAs nanowire field-effect transistors, Sensors 17 (7) (2017) 1640, https://doi.org/10.3390/s17071640.
[20] X. Zhang, M. Fu, X. Li, T. Shi, Z. Ning, X. Wang, T. Yang, Q. Chen, Study on the response of InAs nanowire transistors to H_2O and NO_2, Sens. Actuators B: Chem. 209 (2015) 456–461, https://doi.org/10.1016/j.snb.2014.11.142.
[21] J. Du, D. Liang, H. Tang, X.P.A. Gao, InAs nanowire transistors as gas sensor and the response mechanism, Nano Lett. 9 (12) (2009) 4348–4351, https://doi.org/10.1021/nl902611f.
[22] D. Lynall, A.C. Tseng, S.V. Nair, I.G. Savelyev, M. Blumin, S. Wang, Z.M. Wang, H. E. Ruda, Nonlinear chemical sensitivity enhancement of nanowires in the ultralow concentration regime, ACS Nano 14 (1) (2020) 964–973, https://doi.org/10.1021/acsnano.9b08253.
[23] S.A. Dayeh, Electron transport in indium arsenide nanowires, Semicond. Sci. Technol. 25 (2) (2010) 024004, https://doi.org/10.1088/0268-1242/25/2/024004.
[24] D. Lynall, S.V. Nair, D. Gutstein, A. Shik, I.G. Savelyev, M. Blumin, H.E. Ruda, Surface state dynamics dictating transport in InAs nanowires, Nano Lett. 18 (2) (2018) 1387–1395, https://doi.org/10.1021/acs.nanolett.7b05106.
[25] S. Upadhyay, R. Frederiksen, N. Lloret, L.D. Vico, P. Krogstrup, J.H. Jensen, K. L. Martinez, J. Nygård, Indium arsenide nanowire field-effect transistors for pH and biological sensing, Appl. Phys. Lett. 104 (20) (2014) 203504, https://doi.org/10.1063/1.4878659.
[26] E. Bakker, P. Bühlmann, E. Pretsch, Carrier-based ion-selective electrodes and bulk optodes. 1. General characteristics, Chem. Rev. 97 (8) (1997) 3083–3132, https://doi.org/10.1021/cr940394a.
[27] E. Bakker, P. Bühlmann, E. Pretsch, The phase-boundary potential model, Talanta 63 (1) (2004) 3–20, https://doi.org/10.1016/j.talanta.2003.10.006.
[28] K. Kimura, M. Yoshinaga, K. Funaki, Y. Shibutani, K. Yakabe, T. Shono, M. Kasai, M. Hideya, M. Tanaka, Effects of α-substituents on ion selectivity of bis(12-crown-4-methyl) malonates as neutral carriers for sodium ion-selective electrodes, Anal. Sci. 12 (1) (1996) 67–70, https://doi.org/10.2116/analsci.12.67.
[29] K. Ito, H. Satake, Y. Mori, A.C. Tseng, T. Sakata, Biocompatible and Na^+-sensitive thin-film transistor for biological fluid sensing, Sci. Technol. Adv. Mater. 20 (1) (2019) 917–926, https://doi.org/10.1080/14686996.2019.1656516.
[30] T. Sakata, M. Hagio, A. Saito, Y. Mori, M. Nakao, K. Nishi, Biocompatible and flexible paper-based metal electrode for potentiometric wearable wireless biosensing, Sci. Technol. Adv. Mater. 21 (1) (2020) 379–387, https://doi.org/10.1080/14686996.2020.1777463.
[31] M. Ding, Q. He, G. Wang, H.-C. Cheng, Y. Huang, X. Duan, An on-chip electrical transport spectroscopy approach for in situ monitoring electrochemical interfaces, Nat. Commun. 6 (2015) 7867, https://doi.org/10.1038/ncomms8867.
[32] H. Wang, Y. Wu, C. Cong, J. Shang, T. Yu, Hysteresis of electronic transport in graphene transistors, ACS Nano 4 (12) (2010) 7221–7228, https://doi.org/10.1021/nn101950n.
[33] R.E.G. van Hal, J.C.T. Eijkel, P. Bergveld, A general model to describe the electrostatic potential at electrolyte oxide interfaces, Adv. Colloid Interface Sci. 69 (1–3) (1996) 31–62, https://doi.org/10.1016/s0001-8686(96)00307-7.
[34] H. Braunschweig, I. Krummenacher, L. Mailänder, L. Pentecost, A. Vargas, Formation of a stable radical by oxidation of a tetraorganoborate, Chem. Commun. 52 (3) (2016) 7005–7008, https://doi.org/10.1039/c6cc02916g.
[35] D.H. Geske, Evidence for the formation of biphenyl by intramolecular dimerization in the electroöxidation of tetraphenylborate ion, J. Phys. Chem. 66 (9) (1962) 1743–1744, https://doi.org/10.1021/j100815a507.
[36] V.V. Ilchenko, V.V. Marin, S.D. Lin, K.Y. Panarin, A.A. Buyanin, O.V. Tretyak, Room temperature negative differential capacitance in self-assembled quantum dots, J. Phys. D: Appl. Phys. 41 (23) (2008) 235107, https://doi.org/10.1088/0022-3727/41/23/235107.

[37] A. Kumar, P. Balakrishna Pillai, X. Song, M.M. De Souza, Negative capacitance beyond ferroelectric switches, ACS Appl. Mater. Interfaces 10 (23) (2018) 19812–19819, https://doi.org/10.1021/acsami.8b05093.
[38] D. Lynall, K. Byrne, A. Shik, S.V. Nair, H.E. Ruda, Surface properties from transconductance in nanoscale systems, Nano Lett. 16 (10) (2016) 6028–6035, https://doi.org/10.1021/acs.nanolett.6b01800.
[39] G. Högg, O. Lutze, K. Cammann, Novel membrane material for ion-selective field-effect transistors with extended lifetime and improved selectivity, Anal. Chim. Acta 335 (1–2) (1996) 103–109, https://doi.org/10.1016/s0003-2670(96)00284-x.
[40] M.E. Poplawski, R.B. Brown, K.L. Rho, S.Y. Yun, H.J. Lee, G.S. Cha, K.-J. Paeng, One-component room temperature vulcanizing-type silicone rubber-based sodium-selective membrane electrodes, Anal. Chim. Acta 355 (2–3) (1997) 249–257, https://doi.org/10.1016/s0003-2670(97)00482-0.
[41] T. Sokalski, T. Zwickl, E. Bakker, E. Pretsch, Lowering the detection limit of solvent polymeric ion-selective electrodes. 1. Modeling the influence of steady-state ion fluxes, Anal. Chem. 71 (6) (1999) 1204–1209, https://doi.org/10.1021/ac980944v.

Alex C. Tseng obtained his BASc (2015) and MASc (2018) in Materials Science and Engineering from the University of Toronto. He is currently pursuing his PhD in the same field at The University of Tokyo. Current and past research interests include: gas and aqueous phase sensing using semiconducting nanowires, as well as applications of the thermoelectric and electrochemical properties of conductive polymers and composites.

Kensuke Ito received his BS (2016) and MS (2018) degrees from the Department of Materials Engineering at The University of Tokyo. Heis currently working as a researcher at Fujifilm Corporation, Japan.

David Lynall is currently a Postdoctoral Research Associate in the Bioelectronic Systems Lab at Columbia University. He obtained his BASc (2009) in Electrical Engineering from Purdue University and his PhD (2019) in Materials Science and Engineering from the University of Toronto. Current and past research interests include: chemical and biological sensing using carbon nanotubes and semiconductor nanowires, electron transport phenomena in low-dimensional semiconductors, single-molecule sensing, and ultrasonic transducer circuits for biomedical imaging.

Igor G. Savelyev is currently a senior research associate at the University of Toronto. He received his BSc in experimental physics from Leningrad Politechnical Institute Russia in 1982; his MSc thesis focused on I-V characteristics of the inhomogeneous p-n junctions in GaAs-GaSb systems. His PhD research at the Ioffe Physical Technical Institute, Leningrad, focused on quantum coherent effects in a two-dimensional electron gas. In 2002 he joined the Centre for Advanced Nanotechnology at the University of Toronto, where he is responsible for MBE research on complex semiconductor nanostructure for optoelectronics, with a current focus on controllable heteroepitaxy of semiconductor nanostructures.

Shiliang Wang is a Defence Scientist working at Suffield Research Centre. Defence Research and Development Canada. He obtained his BSc and MSc from Shandong University and Tsinghua University in 1984 and 1987, respectively. In 1987, he joined the Department of Physics in Tsinghua University and was promoted to Lecturer in 1990. He was a visiting scholar at the University of Glasgow under the support of a Royal Society Fellowship Award in 1995. He obtained his PhD from the University of Edinburgh in 1999. His current interest areas are material developments for chemical and biological hazard detection, identification, and protection.

Harry E. Ruda is the Stanley Meek Chair Professor in Nanotechnology at the University of Toronto, and Director of the Centre for Advanced Nanotechnology. After obtaining his BSc (1979) from Imperial College, he joined MIT where he completed his PhD (1982) working on the optical and transport properties of II-VI based infrared detector materials. As an IBM Postdoctoral Fellow (1982-1984) he developed one of the first theories for electron transport in selectively doped two-dimensional electron gas heterostructures. In 1984, he joined 3M Corporation as a senior scientist developing some of the first models for electronic transport and optical properties of wide bandgap II-VI semiconductors. He joined the University of Toronto in 1989, where he rose to a Full Professor appointment. Professor Ruda has published over 290 publications in international refereed journals (with over 7726 citations; h=43), co-authored 4 books, and holds 14 patents. His research topics focus on optoelectronic nanostructures with applications in areas such as biosensing and information technology.

Toshiya Sakata is an Associate Professor in Biosensing Materials and Science at The University of Tokyo. He received his BS (1998), MS (2000), and PhD (2003) from Osaka University. In 2003, he joined the National Institute for Materials Science (NIMS), Tsukuba, as a Researcher working on FET-based DNA sensors. In 2006, he joined the Department of Materials Engineering at The University of Tokyo as a project lecturer. He was promoted to Lecturer in 2008 and again to Associate Professor in 2011. From 2015, he has served as a director of PROVIGATE, Inc., where his biosensing technology has been applied. During 2015-2016, he was a visiting associate professor working on research of chondrocytes-cultured biosensors in the Department of Otrhopaedic Surgery, Brigham and Women's Hospital, at Harvard Medical School. His current research is engaged in the development of semiconductor-based biosensors for health care devices.